THE JOURNAL OF BIOLOGICAL CHEMISTRY
Vol. 274, No. 51, Issue of December 17, pp. 36465–36471, 1999

*Printed in U.S.A.*

# Crystal Structure of β-Ketoacyl-Acyl Carrier Protein Synthase III

## A KEY CONDENSING ENZYME IN BACTERIAL FATTY ACID BIOSYNTHESIS*

(Received for publication, August 4, 1999, and in revised form, August 25, 1999)

**Xiayang Qiu‡, Cheryl A. Janson, Alex K. Konstantinidis, Silas Nwagwu, Carol Silverman, Ward W. Smith, Sanjay Khandekar, John Lonsdale, and Sherin S. Abdel-Meguid**

*From SmithKline Beecham Pharmaceuticals, King of Prussia, Pennsylvania 19406*

**β-Ketoacyl-acyl carrier protein synthase III (FabH), the most divergent member of the family of condensing enzymes, is a key catalyst in bacterial fatty acid biosynthesis and a promising target for novel antibiotics. We report here the crystal structures of FabH determined in the presence and absence of acetyl-CoA. These structures display a fold that is common for condensing enzymes. The observed acetylation of $Cys^{112}$ proves its catalytic role and clearly defines the primer binding pocket. Modeling based on a bound CoA molecule suggests catalytic roles for $His^{244}$ and $Asn^{274}$. The structures provide the molecular basis for FabH substrate specificity and reaction mechanism and are important for structure-based design of novel antibiotics.**

Condensing enzymes catalyze carbon-carbon bond formation by condensing an acyl primer with an elongating carbon source often attached to a holo-acyl carrier protein (ACP).[1] These enzymes act either as single polypeptides or domains of multienzyme complexes. They are responsible for the biosynthesis of a diverse set of natural products, including fatty acids (1, 2) and polyketides (3), and have recently been used to catalyze the synthesis of "unnatural" compounds (4, 5). Three condensing enzymes are involved in bacterial fatty acid biosynthesis: FabB, FabF, and FabH (β-ketoacyl-ACP synthase I, II, and III, respectively). Each catalyzes a distinct biochemical reaction (1, 2). FabH plays a central role in fatty acid synthesis because it catalyzes the initiating condensation reaction and is responsible for the feedback regulation of the pathway via product (palmitoyl-ACP) inhibition (6–9). FabH catalyzes the condensation of acetyl-CoA and malonyl-ACP to yield acetoacetyl-ACP. The reaction is believed to occur in three steps: the acetyl transfer from acetyl-CoA to a catalytic cysteine, the decarboxylation of malonyl-ACP to form a carbanion, and the condensation of the acetyl group and carbanion (1, 2). FabH most likely acts as a homodimer of ~70 kDa (10, 11). In a similar manner to other components of the dissociated (type II) fatty acid synthase system, FabH exists as an isolated enzyme. In vertebrates, however, this enzymatic activity is encoded in the N terminus of a large multi-functional Type I fatty acid synthase, which displays no overall sequence homology to the bacterial enzyme. Emerging resistance to currently used antibacterial agents has generated an urgent need for antibiotics acting via novel mechanisms (12, 13). FabH exists ubiquitously in bacteria and is essential for viability,[2] suggesting it is a potential broad-spectrum antibacterial target. Moreover, thiolactomycin has been shown to be an effective inhibitor of bacterial condensing enzymes; it also possesses antibacterial activity (1, 2). The significant differences between bacterial and human fatty acid synthase systems suggest great potential for specific and selective inhibition. Most condensing enzymes contain a consensus sequence of 45 amino acids, but FabH is the most divergent member of the family and matches few of the consensus residues (14). The antibiotic cerulenin inhibits almost all condensing enzymes but not FabH (15). Thus, FabH could have a fold and evolutionary origin different from other condensing enzymes. Here we report the crystal structure of *Escherichia coli* FabH in the presence and absence of ligand and show that the enzyme contains a quasi-2-fold symmetry, most likely resulting from gene duplication. The structures suggest a conserved fold for all condensing enzymes, provide the structural basis for the catalytic mechanism, and will serve as molecular templates for structure-based drug design.

### EXPERIMENTAL PROCEDURES

*Protein Purification and Crystallization*—Native *E. coli* FabH protein was overexpressed in *E. coli* DH10B cells using the pET29 (Novagen) vector and purified to homogeneity in three chromatographic steps (Q-Sepharose, MonoQ, and hydroxyapatite) at 4 °C. The selenomethionine-substituted protein was expressed in *E. coli* BL21 cells and purified in a similar way. Apo FabH crystals were obtained with the native protein using 20% polyethylene glycol 8000 at neutral pH, whereas the acetyl-CoA complex crystals were obtained with the selenomethionine protein using saturating acetyl-CoA and 14% polyethylene glycol 6000 at neutral pH. Crystals were ~0.3 mm in size and were frozen before data collection.

*Data Collection and Multiple-wavelength Anomalous Dispersion Phasing*—Diffraction data from the apo crystal were measured to 2.0 Å resolution at the Industrial Macromolecular Crystallography Association 17-ID beam line at the Advanced Photon Source (Table I). The crystal was of the orthorhombic $P2_12_12_1$ space group with cell dimensions $a = 63.1$, $b = 65.1$, and $c = 166.5$ Å, with one FabH dimer per asymmetric unit. The selenomethionine FabH·acetyl-CoA complex crystal belongs to the tetragonal space group $P4_12_12$, with $a = b = 72.4$ and $c = 102.8$ Å, and contains a monomer per asymmetric unit. The data (Table I), obtained at the X12C beam line of the Brookhaven National Laboratory, were measured at three wavelengths optimal for Se multiple-wavelength anomalous dispersion phasing experiments. Although the crystal mosaicity was as high as 1.4° (compared with that of 0.7° for the apo crystal) and the data were only 80% complete, the data quality was improved by its high redundancy. The acetyl-CoA complex structure was determined to 1.9-Å resolution using the multiple-wavelength anomalous dispersion phasing technique with the program SOLVE (16). There are 8 methionines in *E. coli* FabH; all were correctly located by SOLVE and refined to reasonable occupancies (0.62–1.00) and tem-

* The costs of publication of this article were defrayed in part by the payment of page charges. This article must therefore be hereby marked "*advertisement*" in accordance with 18 U.S.C. Section 1734 solely to indicate this fact.

*The atomic coordinates and structure factors (code 1D9B) have been deposited in the Protein Data Bank, Research Collaboratory for Structural Bioinformatics, Rutgers University, New Brunswick, NJ (http://www.rcsb.org/).*

‡ To whom correspondence should be addressed. Tel.: 610-270-4589; Fax: 610-270-4091; E-mail: xiayang_qiu-1@sbphrd.com.

[1] The abbreviations used are: ACP, acyl-carrier protein; FabH, β-ketoacyl-ACP synthase III; FabF, β-ketoacyl-ACP synthase II; r.m.s., root mean square.

[2] J. Lonsdale, unpublished data.

TABLE I
*Structure determination and refinement statistics*

Diffraction data

Native

| Resolution | Unique reflections | Total reflections | Redundancy | Complete | $R_{sym}$[a] |
|---|---|---|---|---|---|
| Å | | | | % | |
| 30–2.0 | 50,198 | 292,572 | 5.8 | 97.1 | 0.077 |

Se-Met

| λ | Resolution | Unique/total | Redundancy | % | $R_{sym}$ | $R_{ano}$[b] | $f'_{obs}/f''_{obs}$[c] |
|---|---|---|---|---|---|---|---|
| Å | Å | | | | | | |
| 0.9414 | 30–1.9 | 33,457/195,845 | 5.9 | 81.1 | 0.095 | 0.059 | 3.4/4.2 |
| 0.9785 | 30–1.9 | 33,450/203,786 | 6.0 | 81.2 | 0.083 | 0.074 | −7.5/6.0 |
| 0.9789 | 30–1.9 | 31,992/171,077 | 5.3 | 77.5 | 0.084 | 0.054 | −9.7/3.9 |

MAD phasing

| Resolution (Å) | 30–6.82 | 4.31 | 3.37 | 2.86 | 2.53 | 2.29 | 2.11 | 1.90 | Total |
|---|---|---|---|---|---|---|---|---|---|
| <Figure of merit> | 0.80 | 0.82 | 0.79 | 0.78 | 0.71 | 0.51 | 0.40 | 0.24 | 0.60 |

Refinement

| Resolution | Reflections | Atoms | Waters | $R$[d] | $R_{free}$[e] | r.m.s. bonds | rms angles |
|---|---|---|---|---|---|---|---|
| Å | *n* | *n* | *n* | % | % | Å | ° |
| Apo (native) | | | | | | | |
| 7.0–2.0 | 40,478 | 5,206 | 504 | 18.9 | 24.4 | 0.011 | 2.0 |
| Acetyl-CoA (Se-Met) | | | | | | | |
| 7.0–1.9 | 15,890 | 2,591 | 189 | 26.0 | 30.4 | 0.014 | 2.3 |

[a] $R_{sym} = \Sigma\,|I - \langle I\rangle|/\Sigma$I, where $I$ is the intensity of an observed reflection, and $\langle I\rangle$ is the average intensity of reflections related to $I$ by symmetry. Friedel mates were counted separately in the number of unique reflections.
[b] $R_{ano} = \Sigma\,|I^+ - I^-|/\Sigma\langle I\rangle$, where $I^+$ and $I^-$ are the Friedel mates, and $\langle I\rangle$ is the average of their intensity.
[c] Observed mean $f'$ and $f''$ scattering factors in number of electrons.
[d] $R = \Sigma||F^{obs}| - |F^{cal}||/\Sigma|F^{obs}|$.
[e] $R_{free} = \Sigma||F^{obs}| - |F^{cal}||/\Sigma|F^{obs}|$, where $F^{obs}$ is from a test set of reflections (5% of the total) that are not used in structural refinement.

perature factors (23 -41 Å$^2$). The overall figure of merit was 0.6 from 30 to 1.9 Å resolutions, and the overall $Z$ score was 148. The resulting electron density map was of very high quality (Fig. 1).

*Model Building and Refinement*—The whole FabH protein (317 residues), the bound acetyl and CoA, as well as 98 solvent molecules were built in the initial model. The data set collected at the inflection point wavelength (0.9785) ($I > 2\sigma[I]$) were used for structural refinement with XPLOR (17) because its completion is the highest among the three. The apo FabH structure ($P2_12_12_1$) was solved using the molecular replacement program AMORE (18) with the protein atoms from the acetyl-CoA complex structure as the search model. The two monomers were identified, and the solution gave an $R$-factor of 33% (8.0–3.5 Å). The model was initially built using the 2-fold averaged electron density map and refined to the final model using XPLOR. Both models (Table I) have good geometry with no Ramachandran outliers. The apo structure is clearly of good quality, as indicated by the low $R$-factors; the acetyl-CoA complex structure is also valid for the discussions in this report. This is because the high-quality electron density map (Fig. 1) is calculated from experimental phases; the complex structure has been used successfully to solve the apo structure; and the two structures are practically the same at α-carbon level (r.m.s., 0.3 Å). We have not included the Se atoms and their anomalous signal in the current stage of refinement, resulting in the slightly higher $R$-factors of the complex structure. The figures were created with the computer programs XTALVIEW (19), MOLSCRIPT (20), and GRASP (21).

## RESULTS

*Overall Structure: E. coli*—FabH displays a five-layered core structure, α-β-α-β-α, where each α comprises two α-helices and each β is made of a five-stranded, mixed β-sheet (Fig. 2*A*). Despite the lack of overall sequence homology, the FabH core structure is similar to that of FabF, the other condensing enzyme of known structure (22, 23). This fold was first identified in thiolase I, which catalyzes the degradation of ketoacyl-CoA structure (24, 25). The superposition of the FabH and FabF cores results in a r.m.s. difference of 1.7 Å for 160 pairs of α-carbon atoms. In the comparison, Na2, Ca2, Cb3, and part of Ca3 were excluded because of large differences. The structures beyond the cores fold into a domain for substrate recognition (Fig. 2*A*) and intermolecular interactions, and this domain is completely unrelated to that of FabF or thiolase. The overall sequence identity is only 14% between FabH and FabF, but the 160 pairs of structurally matched residues have a higher sequence identity of 21%, indicating that FabH is evolutionally related to FabF. Because FabF fits well with the consensus sequence (14), our results suggest a common ancestor for all condensing enzymes. Their sequences and peripheral structures have diverged significantly throughout evolution to accommodate the differences in substrates. The FabH monomer appears to have been generated through gene duplication. The two halves, residues 1–170 and 171–317, have only 11% overall sequence identity. However, their structures are similar except for the insertion and loop regions (Fig. 2*B*). The best matched structural elements of the two FabH halves are strands b1, b2, b4, and b5. Within these strands, the 33 pairs of α-carbons can be superimposed with a r.m.s. difference of only 1.0 Å, and the sequence identity between them is as high as 24%. A search of sequence data bases revealed no homologous proteins half the size of FabH, except for a few hypothetical proteins deduced from DNA sequences.

*Structure of the Dimer*—The crystal structure of FabH revealed the presence of a tight dimer (Fig. 3), consistent with our biochemical data[3] and similar to the structures of FabF (22, 23) and thiolase I (24, 25). The dimer interface mainly involves Nb3, Na3, and Na2 and buries ~2670 Å$^2$ of accessible surface area. Strand Nb3 of one monomer interacts with that of the other monomer to form a continuous 10-stranded β-sheet in the dimer. Helix Na3, with the catalytic $Cys^{112}$ near its N terminus ($Gly^{114}$), uses its C-terminal half to interact with its counterpart from the other monomer. This suggests that the dimer

[3] A. Konstandinidis, unpublished data.

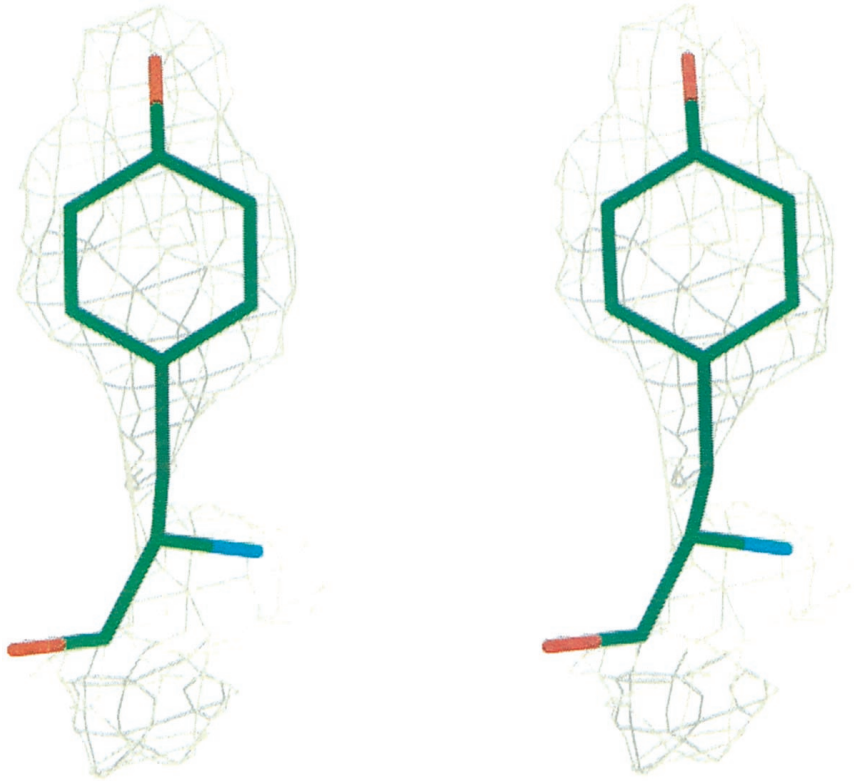

FIG. 1. **Experimentally (MAD) phased electron density map at Tyr$^{125}$ in a cross-eye stereo view.** The map is contoured at 1.5 $\sigma$, and Tyr$^{125}$ is from the refined model. The extra electron density near the main chain atoms of Tyr$^{125}$ belongs to the backbone atoms of the neighboring residues.

interface is important for positioning the catalytic apparatus of FabH. The two active sites, facing opposite sides in the dimer, are formed mostly by residues within each monomer. However, Phe87 (in a loop preceding helix Na2) of one monomer projects into the active site of the other monomer. These structural features suggest that the observed dimer is the biologically relevant structure, and that its formation is essential for the proper functioning of the FabH enzyme.

*Catalytic Residues*—Each FabH active site, located at the center of the monomer, is formed at the interface of the N- and C-terminal domains (Fig. 2*A*). The catalytic residues in thiolase I were proposed to be Cys$^{125}$, His$^{375}$, and Cys$^{403}$ (24, 25), whereas those in FabF were predicted to be Cys$^{163}$, His$^{303}$, and His$^{340}$ (22, 23). The corresponding residues in FabH were found by structural alignment to be Cys$^{112}$, His$^{244}$, and Asn$^{274}$. Although FabH Cys$^{112}$ aligns well with Cys$^{163}$ of FabF and Cys$^{125}$ of thiolase I, the structural superposition revealed significant differences among other catalytic residues (Fig. 4). The lack of a Cys$^{403}$-like residue in FabH implies a role for that residue that is relevant only to the thiolase reaction. Asn$^{274}$ superimposes well with the histidines in FabF (His$^{340}$) and thiolase I (His$^{375}$), but His$^{244}$ is far from its counterpart (His$^{303}$) in FabF, suggesting different substrate specificity. A previously unsuspected thiolase residue, Asn$^{343}$, is found near His$^{244}$ of FabH. If Asn$^{343}$ plays a role in catalysis, it is possible that the His-Asn pairs of FabH and thiolase are inverted structurally to match the reversed reactions they catalyze.

*Substrate or Ligand Binding*—Both FabF and thiolase I structures were determined in the absence of a substrate; thus, the structural basis for catalysis and substrate specificity has not been established. To further investigate these important questions, we co-crystallized FabH with its first substrate, acetyl-CoA. The overall structure of FabH in the acetyl-CoA complex agrees well with the apo structure, with a r.m.s. difference of 0.3 Å for all 317 $\alpha$-carbons. The electron density reveals a covalent attachment of the acetyl moiety to Cys$^{112}$ (bond distance, 1.8 Å), indicating that the substrate was turned over by the enzyme to yield an initial product complex. This is direct evidence that Cys$^{112}$ is the catalytic nucleophile. The acetyl oxygen makes hydrogen bonds to the backbone nitrogens of Gly$^{306}$ (2.8 Å) and Cys$^{112}$ (3.0 Å). These backbone nitrogens are ideal for stabilizing the oxyanion formed during the transition state of acetyl transfer. The same role can be suggested for the backbone nitrogens of Phe$^{400}$ and Cys$^{163}$ of FabF by structural analogy. FabH Ala$^{113}$ has a slightly unfavorable torsion angle, which may be required to make Cys$^{112}$ N available for the interaction. The acetyl methyl group occupies a hydrophobic pocket in the active site, formed by the side chains of Leu$^{142}$, Phe$^{157}$, Leu$^{189}$, Leu$^{205}$, and Phe$^{87'}$, which belongs to the other monomer (Fig. 5*A*). The van der Waals interactions between the acetyl methyl and Phe$^{87'}$ suggest that the dimer interface plays a critical role in determining the primer specificity of FabH.

Surprisingly, we found a CoA molecule bound in the acetyl-CoA complex, although the electron density is weak for parts of the molecule (Fig. 5*B*). Observing CoA in the crystal suggests that the reaction product has a notable FabH affinity. The bound CoA allows us to define the active site cavity, which is long (~15 Å) and narrow, ideal for fitting the pantetheine group of substrates in a more or less extended conformation. The adenine ring of CoA stacks between the side chains of Trp$^{32}$ and Arg$^{151}$ (Fig. 5*C*), a classical adenine binding mode. The Arg$^{151}$ side chain also interacts with the ribose hydroxyl (3.4 Å) and phosphate (3.2 Å), whereas the N-cap dipole of helix Cb1 and Arg$^{36}$ are involved in stabilizing the diphosphate. The pantetheine group interacts with the hydrophobic wall of the active site cavity, comprised of residues such as Ile$^{156}$, Met$^{207}$, Val$^{212}$, Phe$^{213}$, and Ile$^{250}$. The pantothenate also forms a couple of hydrogen bonds (O9 to Asn$^{247}$ ND2, 2.9 Å; N8 to Gly$^{209}$ O, 3.1 Å) with the enzyme, but the $\beta$-mercaptoethylamine tail of CoA is flexible, as indicated by the weak electron density and the lack of specific protein interactions. Cys$^{112}$ is at the bottom of this cavity, with the acetyl carbon 3.9 Å away from the CoA sulfur atom (Fig. 5*A*).

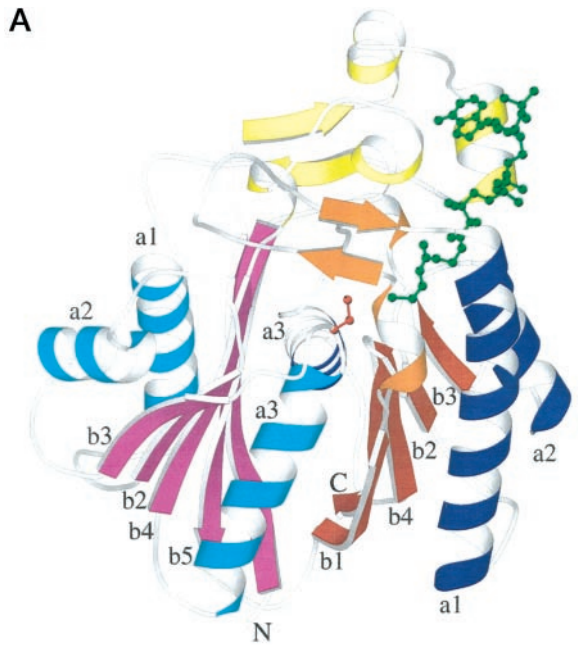


FIG. 2. **Overall structure of *E. coli* FabH.** *A*, ribbon diagram of the FabH monomer. The N-terminal (1–170) and C-terminal (171–317) halves have a similar fold. The core secondary structural elements are labeled as *b1–b5* and *a1–a3*, respectively and referred in the text with a prefix of *N* or *C* to indicate the domain they belong to. These β-sheet and α-helices are drawn in *magenta* (*N, b1–b5*), *cyan* (*N, a1–a3*), *red* (*C, b1–b5*), and *blue* (*C, a1–a3*). *N* is the N terminus, which precedes *N, b1*. *C* is the C terminus, which comes off *C, b5*. Secondary elements of insertion regions are drawn in *yellow* and *orange* for N- and C-terminal domains, respectively. The catalytic $Cys^{112}$ is shown in a *red ball-and-stick drawing*, and the CoA molecule (*green*) was taken from the acetyl-CoA complex structure to orient the view. *B*, stereo view of the superposition between the N-terminal (*red*) and C-terminal (*blue*) domains of FabH. Core β-strands are labeled; the overlay was generated by matching the 33 α-carbon pairs from four of the strands.

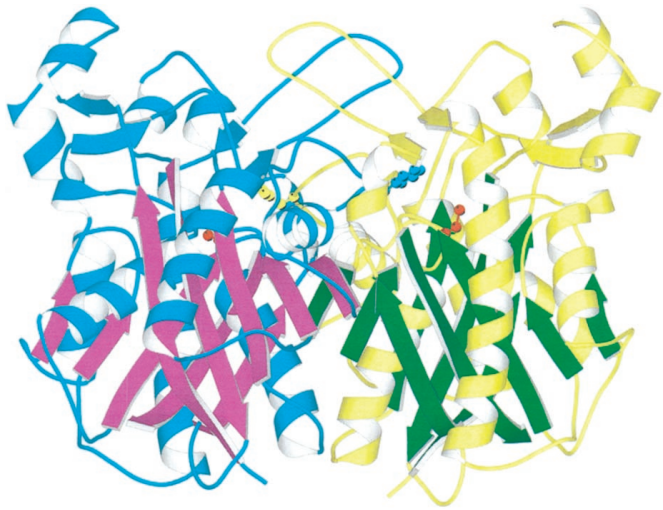

FIG. 3. **Ribbon diagram of the FabH dimer.** The dimer is viewed perpendicular to the two-fold axis. One monomer is shown in *yellow* and *green*; the other is shown in *cyan* and *magenta*. $Phe^{87}$ and $Cys^{112}$ (*red*) are shown as *ball-and-stick models*.

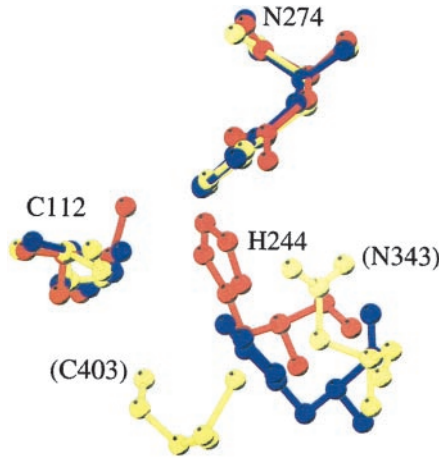


FIG. 4. **Superposition of potential catalytic residues in FabH (*red*), FabF (*blue*), and thiolase I (*yellow*).** FabH residues are labeled. The corresponding residues in FabF are $Cys^{163}$, $His^{303}$, and $His^{340}$, and those in thiolase are $Cys^{125}$, $Asn^{343}$, $His^{375}$, and $Cys^{403}$. Thiolase $Asn^{343}$ and $Cys^{403}$ are labeled in *parentheses*.

## DISCUSSION

It has been shown that FabH can accept primers such as acetyl-, propionyl-, and butyryl-CoA, but not long chain acyl-CoA (7, 8). This is supported by our FabH structure, in which the primer binding pocket is indeed quite small (Fig. 5*A*). The acetyl methyl group takes up most of the space in this pocket and is within reasonable van der Waals distances to $Leu^{142}$, $Phe^{157}$, and $Phe^{87\prime}$. It is possible to model an additional carbon pointing between the side chains of $Leu^{189}$ and $Phe^{157}$, suggesting a propionyl group can also fit. Adding yet another carbon appears to require side chain rearrangements, consistent with a much reduced efficiency for butyryl-CoA. This is in contrast to the FabF primer binding pocket that is much more extended and is the locus of binding of cerulenin (23). A helical segment of FabF ($Phe^{133}$-$Ile^{138}$) is found by structural analogy to play a role similar to FabH $Phe^{87\prime}$, suggesting the use of dimer interface as a conserved feature in condensing enzymes to modulate primer specificity. It is clear from structural inspection that cerulenin or a long acyl chain would not bind the FabH enzyme because the pocket is too small.

Although our acetyl-CoA structure turns out to be a product complex, the observed CoA provides a basis for modeling either of the FabH substrates. As indicated by the nature of the interactions, the mode of CoA binding should approximate that of the acetyl-CoA from adenine to most of the pantothenate. The observed flexible CoA tail is probably not an accurate representation of acetyl-CoA, but the substrate binding mode can be modeled with only a few free bond rotations. In such a model, this tail is probably in a more extended conformation. The hydrogen bonds between the acetyl carbonyl oxygen and the backbone nitrogens of $Gly^{306}$ and $Cys^{112}$ may guide the acetyl group into the active site, positioning it for nucleophilic attack by $Cys^{112}$ (Fig. 6*A*). $His^{244}$, 3.4 Å from $Cys^{112}$, is in position to act as a general base and extract a proton from

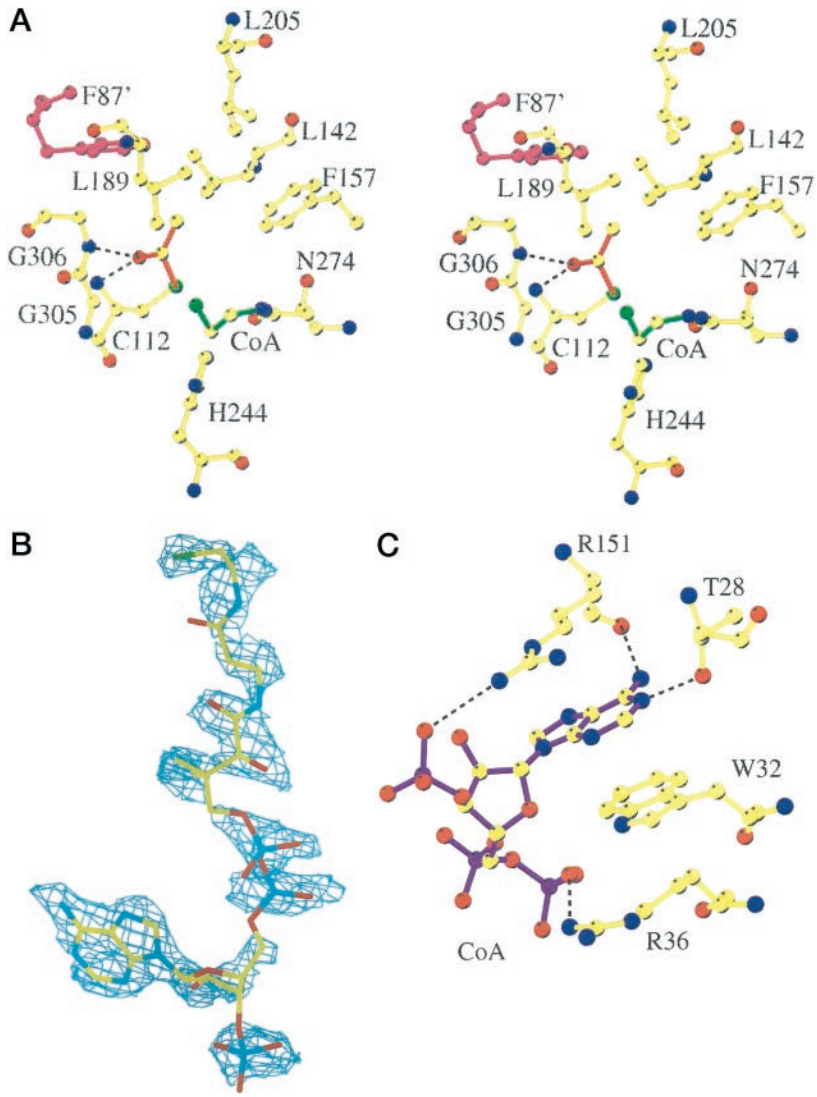


FIG. 5. **Substrate binding and structure of the active site.** *A*, stereo view of the acetyl binding pocket in the active site. Atom colors are as defined as follows: carbon, *yellow*; nitrogen, *blue*; oxygen, *red*; and sulfur, *green*. The acetyl group is shown with *red* bonds, whereas the *dashed lines* indicate hydrogen bonds. $Phe^{87}$ of the other monomer in the FabH dimer is labeled as $Phe^{87'}$ and is shown in *magenta*. For clarity, only the mercaptoethylamine group of CoA is shown, which is drawn with *green* bonds. *B*, electron density of the bound CoA molecule. Atom colors are as defined before, with the three phosphorous atoms in *blue* as well. The map is contoured at 1$\sigma$. *C*, adenine binding site. Protein residues are in *yellow* bonds, and the CoA molecule is drawn in *purple* bonds. Carbon atoms are drawn in *yellow*, nitrogens in *blue*, oxygens in *red*, and phosphors in *purple*. The *dashed lines* denote hydrogen bonds.

$Cys^{112}$. $Asn^{274}$ is too far (4.2 Å from $Cys^{112}$) to assume this role. The side chain of $Ser^{276}$ is 3.8 Å from $Cys^{112}$, but its nature prohibits it from accepting a proton. The reaction likely goes through a tetrahedral intermediate, with the carbonyl group forming an oxyanion. The backbone nitrogens of $Gly^{306}$ and $Cys^{112}$ can stabilize this oxyanion. After the acetyl transfer to $Cys^{112}$, $His^{244}$ could replenish the CoA sulfur with a proton to produce a neutral CoA (Fig. 6*A*). In well-known examples such as serine proteases, catalytic residues can be superimposed regardless of large differences in the overall protein folding (26). However, $His^{244}$ and its analogous residue in FabF ($His^{303}$) are in different positions with respect to the catalytic cysteines (Fig. 4). This is most likely attributable to differences in the substrates, suggesting that the histidine may interact directly with substrates or intermediates in addition to its role as the catalytic base. The positional differences in the catalytic apparatus suggest that condensing enzymes are under stringent evolutionary pressure to recognize and process different substrates, another reason for their sequence divergence.

The observed active site cavity appears to be the only access to $Cys^{112}$ and, therefore, the possible binding cavity for the second substrate malonyl-ACP and the feedback inhibitor palmitoyl-ACP. Malonyl-ACP is a common substrate for many condensing enzymes. The phosphopantetheine group is linked to a serine of the ACP, which is an acidic protein of 78 residues (27). A region above the FabH cavity is positively charged and seems to be suitable for ACP binding (Fig. 6*B*). This region mainly includes two helices (Ca1 and Ca2) and contains several positively charged residues ($Arg^{36}$, $Arg^{40}$, $Lys^{214}$, $His^{222}$, $Arg^{235}$, $Arg^{249}$, $Lys^{256}$, and $Lys^{257}$). Binding of the prosthetic group of malonyl-ACP may be modeled based on the bound CoA. This is reasonable given that the acetylated FabH is known to react with ACP to produce acetyl-ACP (6), which is the reverse of the acetyl transfer reaction and a good indication that CoA and ACP can bind FabH similarly in the pantothenate region.

The acetyl transfer reaction is clearly a distinct step in the FabH reaction. A stepwise mechanism has also been proposed for decarboxylation and condensation (14, 28). FabH can catalyze the production of acetyl-ACP from butyryl-CoA and malonyl-ACP (8), further suggesting that decarboxylation need not occur in concert with condensation. The active sites are very similar between the apo and acetylated structures; only $His^{244}$ shifts marginally (0.5 Å). However, it is known that malonyl-ACP only binds acetylated FabH but not the apo form of the enzyme (7, 8). This suggests that either the acetyl group interacts directly with the malonyl moiety, or the change of $Cys^{112}$ electrostatic potential upon acetylation is important for the binding of this substrate. The former is unlikely because iodoacetamide can also induce the binding of the malonyl group (29). The latter is probably true because $His^{244}$ is counterbalanced by $Cys^{112}$ in apo FabH (Fig. 6*A*) but is available in

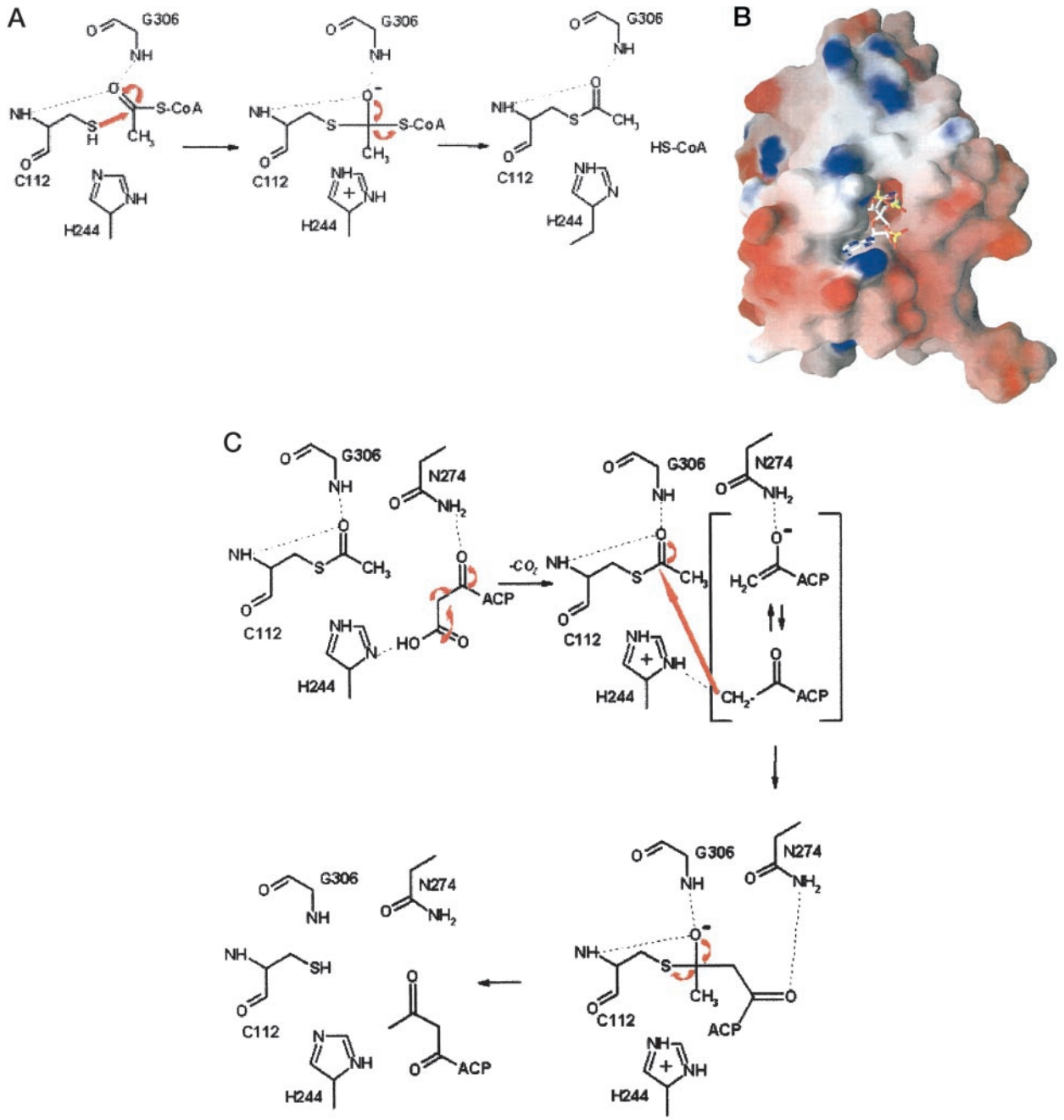


FIG. 6. **Proposed mechanism of the FabH reactions.** *A*, schematic diagram of the acetylation reaction mechanism. *Dotted lines* indicate hydrogen bonds; *thick arrows* indicate attack or electron transfer directions. $His^{244}$ extracts a proton from $Cys^{112}$, which may then attack the carbonyl of acetyl-CoA. The tetrahedral intermediate is stabilized by backbone nitrogens of $Gly^{306}$ and $Cys^{112}$. $His^{244}$ may donate a proton at the end of acetylation to form a neutral CoA. *B*, FabH surface charge distribution viewed toward the active site cavity. The figure was calculated with the acetyl-CoA complex structure after removing the bound CoA. Only the monomer was used, because the dimer interface is not in the area of interest. *Red* indicates negative potential, and *blue* indicates positive potential. The CoA molecule is shown to occupy the active site, with *white* for carbon atoms, *blue* for nitrogens, *red* for oxygens, *yellow* for phosphors, and *green* for the sulfur. *C*, proposed structural basis for the decarboxylation and condensation mechanisms. According to the mechanism (14), the carboxylic acid moiety probably binds $His^{244}$, whereas the carbonyl group interacts with $Asn^{274}$. The decarboxylation produces a carbanion, which resonates with an enol intermediate that is stabilized by $Asn^{274}$. The nucleophilic attack from the carbanion to the enzyme-bound acetyl group leads to a tetrahedral intermediate and finally yields the product acetoacetyl-ACP.

acetylated FabH for a charged interaction with the malonyl carboxylic acid (Fig. 6*C*). $His^{244}$ is the only potentially positively charged residue in the active site, which provides another reason for the proposed $His^{244}$-carboxylic acid interaction during decarboxylation. In addition, $His^{244}$ may stabilize the carbanion for the nucleophilic attack and donate a proton to $Cys^{112}$ after condensation. Modeling clearly suggests that $Asn^{274}$ forms a hydrogen bond with the malonyl carbonyl oxygen. Therefore, $Asn^{274}$ may promote decarboxylation by general acid catalysis via stabilizing an enol intermediate (Fig. 6*C*) and hold the carbanion for nucleophilic attack in condensation. Other condensing enzymes use a histidine in that position, and the histidine is suitable to play these same roles of $Asn^{274}$. Based on our structures, mutagenesis and biochemical experiments can be devised to test these models and their application in other condensing enzymes. The structure will also facilitate the structure-based design of novel antibiotic drugs against this important target.

*Acknowledgments*—We thank the Advanced Photon Source Industrial Macromolecular Crystallography Association-Collaborative Access Team staff and the National Synchrotron Light Source X12C staff for assistance in data collection, Kathleen Maley for help in *E. coli* transformation, Dean McNulty for N-terminal sequence analysis, Dr. David Tew for insightful discussions, and Drs. Robert Daines, Bill Kingsbury, Marti Head, John Elliot, John Gleason, Christine Debouck, Jim Kane, and Glen Van Aller for encouragement.

REFERENCES

1. Cronan, J. E., Jr., and Rock C. O. (1996) in *E. coli and Salmonella, Cellular and Molecular Biology* (Neidhardt, F. C., ed) pp.612–638, ASM Press, Washington, D. C.
2. Magnuson, K., Jackowski, S., Rock, C. O., and Cronan, J. E. (1993) *Microbiol. Rev.* **57,** 522–542
3. Hopwood, D. A., and Sherman, D. H. (1990) *Annu. Rev. Genet.* **24,** 37–66
4. Cane, D. E., Walsh, C. T., and Khosla, C. (1998) *Science* **282,** 63–68
5. McDaniel, R., Thamchaipenet, A., Gustafsson, C., Fu, H., Betlach, M., and Ashley, G. (1999) *Proc. Natl. Acad. Sci. U. S. A.* **96,** 1846–1851
6. Tsay, J. T., Oh, W., Larson, T. J., Jakowski, S., and Rock, C. O. (1992) *J. Biol. Chem.* **267,** 6807–6814
7. Heath, R. J., and Rock, C. O. (1996) *J. Biol. Chem.* **271,** 1833–1836
8. Heath, R. J., and Rock, C. O. (1996) *J. Biol. Chem.* **271,** 10996–11000
9. Verwoert, I. I., van der Linden, K. H., Walsh, M. C., Nijkamp, H. J., and Stuitje, A. R. (1995) *Plant Mol. Biol.* **27,** 875–876
10. Han, L., Lobo, S., and Reynolds, K. A. (1998) *J. Bacteriol.* **180,** 4481–4486
11. Clough, R. C., Matthis, A. L., Barnum, S. R., and Jaworski, J. G. (1992) *J. Biol. Chem.* **267,** 20992–20998
12. Travis, J. (1994) *Science* **264,** 360–362
13. Stinson, S. C. (1996) *Chem. Eng. News* **74,** 75–100
14. Siggaard-Anderson, M. (1993) *Protein Seq. Data Anal.* **5,** 325–335
15. Omura, S. (1979) *Bacteriol. Rev.* **40,** 681–697
16. Terwilliger, T. C., and Berendzen, J. (1999) *Acta Crystallogr.* **D 55,** 849–861
17. Brunger, A. T. (1993) *X-PLOR Version 3.1, A System for X-ray Crystallography and NMR*, Yale University Press, New Haven
18. Collaborative Computational Project Number 4 (1994) *Acta Cryst.* **D 50,** 760–763
19. McRee, D. E. (1993) *Practical Protein Crystallography*, Academic Press, San Diego
20. Kraulis, P. (1991) *J. Appl. Crystallogr.* **24,** 946–950
21. Nicholls, A., and Honig, B. H. (1991) *J. Comp. Chem.* **12,** 435–445
22. Huang, W., Jia, J., Edwards, P., Dehesh, K., Schneider, G., and Lindqvist, Y. (1998) *EMBO J.* **17,** 1183–1191
23. Moche, M., Schneider, G., Edwards, P., Dehesh, K., and Lindqvist, Y. (1999) *J. Biol. Chem.* **274,** 6031–6034
24. Mathieu, M., Zeelen, J. P., Pauptit, R. A., Erdmann, R., Kunau, W. H., and Wierenga, R. K. (1994) *Structure* **2,** 797–808
25. Mathieu, M., Modis, Y., Zeelen, J. P., Engel, C. K., Abagyan, R. A., Ahlberg, A., Rasmussen, B., Lamzin, V. S., Kunau, W. H., and Wierenga, R. K. (1997) *J. Mol. Biol.* **273,** 714–728
26. Qiu, X., Culp, J. S., DiLella, A. G., Hellmig, B., Hoog, S. S., Janson, C. A., Smith, W. W., and Abdel-Meguid S. S. (1996) *Nature* **383,** 275–279
27. Mayo, K. H., and Prestegard, J. H. (1985) *Biochemistry* **24,** 7834–7838
28. Clark, J. D., O'Keefe, S. J., and Knowles, J. R. (1988) *Biochemistry* **27,** 5961–5971
29. Kresze, G. B., Steber, L., Oesterhelt, D., and Lynen, F. (1977) *Eur. J. Biochem.* **79,** 191–199